Defect and Diffusion Forum
ISSN: 1662-9507, Vol. 451, pp 23-33
doi:10.4028/p-nPf0F3

Submitted: 2025-12-17
Accepted: 2026-02-25
Online: 2026-04-17

Influence of Surface Finish and Energy Director on Ultrasonic Welding Process of PAEK/Metal Hybrid Structures

KORYCKI Adrian[1,a*], BEGUIN Jean-Denis[1,b], CHABERT France[1,c] and GARNIER Christian[1,d]

[1]LGP-ENIT-UTTOP, 47 Avenue d'Azereix, 65016 Tarbes, France

[a]adrian.korycki@uttop.fr, [b]jean-denis.beguin@uttop.fr, [c]france.chabert@uttop.fr and [d]christian.garnier@uttop.fr

Keywords: ultrasonic welding, thermoplastic composites, hybrid structure joining, properties

Abstract. The demand for lightweight, multifunctional, and durable hybrid structures is rapidly increasing in aerospace, biomedical, and advanced engineering sectors. Ultrasonic welding (USW) offers a promising route to assemble thermoplastic polymers with dissimilar materials such as stainless steel, aluminium, and ceramics, without adhesives or additional fasteners. This study investigates the ultrasonic joining of high-performance thermoplastics, including carbon fibre-reinforced polyetheretherketone (PEEK), and polyetherimide (PEI) as energy director (ED), with aluminium alloys. Improvement of manufacturing efficiency and weld attributes such as welded area, strength, and failure mechanisms are essential for industrial adoption. In this work, particular attention was given to the effect of metal surface preparation and ED film on weld quality. Weld attributes were analysed in terms of joint area continuity, interfacial morphology, tensile shear strength, and observed failure modes. Whereas not all parameter sets led to successful joining, the findings provide insight into the role of surface finish and ED in determining weldability. These results contribute to the ongoing development of reliable welding for hybrid joining between thermoplastics and metals, highlighting opportunities for thermal process innovation beyond conventional approaches.

Introduction

The development of hybrid metal-polymer structures is part of an innovation strategy for high-value-added sectors such as aerospace, biomedical, and electronics. Ultrasonic welding is a promising method for joining thermoplastics with dissimilar materials due to its speed, low energy consumption and overall low environmental impact. This process uses high-frequency ultrasonic vibrations to generate friction between material, localizing heat at the material interface, enabling fusion and subsequent joining without the need for additional adhesives or time costly surface treatments. Joining dissimilar materials presents unique challenges due to differences in melting temperatures, thermal conductivity, and mechanical properties, which can lead to interfacial stresses and variations in weld quality. Recent advances in controlling the parameters of the ultrasonic welding process [1] are significant assets that allow for improved weld quality and optimized joint strength, durability, and material compatibility. A critical factor in concentrating heat in the weld area is the energy director, with previous research works showing that the ED's thickness and roughness significantly influence the final assembly quality [2], [3]. This work aims to apply this technique for welding high-performance thermoplastic composites and metallic substrates.

The polymers to be welded must combine high thermal resistance, suitable rheological properties, and chemical compatibility with the substrates. Thermoplastic composites with high-performance PAEK (polyaryletherketones) matrix offer an alternative to metals due to similar specific strength. They are already used in aerospace and biomedical sectors due to their excellent mechanical properties, corrosion resistance, radio transparency, and biocompatibility. One of them is polyetheretherketone (PEEK), a semi-crystalline polymer with a melting point of 343°C and excellent mechanical and chemical resistance. Its welding requires precise control of crystallinity [4], [5]. Polyetherketoneketone (PEKK) has a lower melting point of 305-335°C and is easier to weld [6], [7]

due to adjustable kinetics of crystallization. Next, polyetherimide, an amorphous polymer, offers a glass transition temperature of 215°C [8], [9].

Some works on ultrasonic metal-polymer welding are found in the literature They demonstrate that metal surface treatments such as sandblasting, chemical pickling, coating spraying, or mechanical texturing are effective methods for improving the mechanical properties of the joints (AA6061-PA6). The surface roughness of the Al samples is also essential for the weldability. If the roughness is too low, the parts slip on each other. For too high roughness, the energy is transferred in few points in the welding zone. Wagner et al. [10] reported that for ultrasonic welds, a surface roughness in the range 0.2 μm to 5 μm is well suited. However, the impact of treatments varies significantly depending on the nature of materials, which explains the substantial variability in weld strength of approximately 14 MPa [11], [12]. Ultrasonic welding of ABS (acrylonitrile butadiene styrene) to a laser-textured 5052 aluminum sheet was performed by Tan et al. [13]. It was observed that the type of laser texture had a significant influence on the mechanical strength of the joint. At constant laser energy per unit area, the maximum strength of the joint obtained reached 18 MPa in the case of a square grid structure with a 0.1 mm pitch. The welding times were consistently less than 4 s, demonstrating the speed of the process [14]. Compared with other conventional assembly processes like induction welding, resistance welding, friction stir spot welding or even direct adhesive bonding, the ultrasonic metal-polymer welding has proven superior with average shear strength 30 MPa for as-received joints and 50 MPa after surface treatment [15].

The experimental work focuses on the mechanical surface preparation methods for aluminium alloys and the role of PEI as energy director in enhancing joint integrity. Surface modifications allow precise control of roughness and superficial texture. Process parameters such as amplitude, welding time, and applied pressure were optimized and monitored via time and displacement control mode. A new method using multimode ultrasonic welding was tested. The study highlights the critical influence of interfacial morphology, thermal management, and energy director design on joint performance. These findings contribute to the development of reliable ultrasonic welding strategies for metal-polymer hybrid structures.

Materials and Methods

Materials

The thermoplastic composite material utilized in this study was 3106-PA1 five-harness satin weave prepreg, composed of carbon fiber-reinforced polyetherketoneketone (CF/PEKK), supplied by Porcher Industries.

Aluminium sheets of AA5083-H111 alloy with a thickness of 2 mm were also used. Magnesium is the major alloying element in this alloy. The average chemical composition of the aluminium sheet was determined using an oxford-Cegelec FOUNDRY-MASTER spark OES spectrometer, Table 1.

Table 1. Average chemical composition of aluminum sheets (in wt.%)

	Mg	Si	Cu	Fe	Mn	Zn	Cr	Ti	Al
AA5083	3.990 ±0.080	0.200 ±0.004	0.004 ±0.003	0.200 ±0.003	0.390 ±0.008	0.010 ±0.001	0.090 ±0.002	0.010 ±0.001	Bal.

A 0.25 mm thick polyetherimide (PEI) film, provided by Goodfellow, was used as the energy director. PEI was dried at least 24 h at 130°C before welding.

Polymer specimens' preparation

The composite laminates, comprising seven semi-impregnated fabric layers arranged in a [0/90] stacking sequence, were consolidated using a Pinette Emidecau Industries Lab800 thermo-compression device. The CF/PEKK plies were consolidated within a steel frame to reach 2 mm thick plates [16]. Specimens were prepared in dimensions of 100 × 25 mm^2. The edges were deburred after cutting, and all samples were cleaned with ethanol to remove impurities and residual release agents.

Metal surface preparation

Aluminum sheets were cut using laser processing to ensure precise edges for joint configuration welding. After cutting, the weld samples (100 × 25 mm^2) were polished using P300 abrasive silicon carbide (SiC) paper to remove surface oxides and then cleaned with alcohol.

Several types of surface preparation were tested:

- Rough polishing with P60 paper SiC.
- Laser texturing.
- Anodizing.

All pretreated AA5083 substrate was cleaned with acetone and alcohol before and after surface preparation, to remove greasy dirt and aluminum alloy residues using an ultrasonic cleaner.

Laser texture processing was carried out under argon gas protection or atmospheric atmosphere, using a continuous-wave Yb: YAG laser disk (TRUMPF TruDisk 3001), producing periodic grid patterns on surfaces. The texturing area measured 25 x 25 mm^2 and had a spacing interval of 1.5 mm. The laser energy was kept constant by controlling the output power at 500 W, the scan velocity at 75 $mm \cdot s^{-1}$ and the spot size diameter at 200 µm.

The anodizing process for the AA5083 samples was performed in the following steps:

1. Degreasing with acetone.
2. Chemical stripping in 60 $g \cdot l^{-1}$ sodium hydroxides (NaOH).
3. Neutralization in 200 $g \cdot l^{-1}$ nitric acid (HNO_3).
4. Anodizing in an electrolytic solution of 100 $g \cdot l^{-1}$ sulfuric acid (H_2SO_4) for 20 minutes at 20°C with an operating voltage of 18 V and a current density of 2 $A \cdot dm^{-2}$.
5. Rinsing with deionized water and air drying

Experimental methods

Omega 4X ultrasonic welder from Mecasonic was used for the experiments. Its specifications are a working frequency of 20 kHz and a maximum load of 2600 N. The displacement amplitude of the waves generated by the generator is increased by a factor of 1.7 through the booster and further amplified by a factor of 1.7. The welder's sensors and actuators are connected to an interface card located inside the module. Configuration for ultrasonic welding with 40 mm diameter sonotrode is presented in Fig. 1.

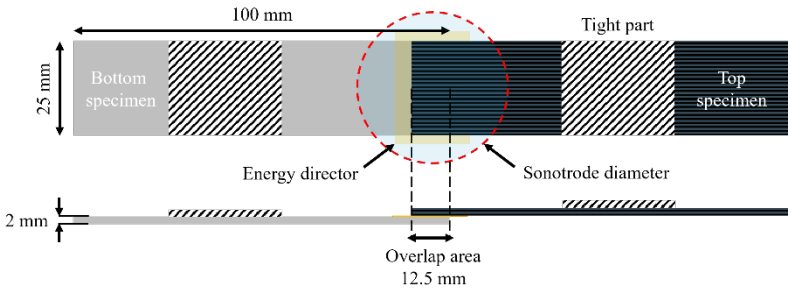

Fig. 1. Scheme showing configuration for USW with 40 mm diameter sonotrode of studied assemblies

The quality of the assemblies was assessed by lap shear strength (LSS). The assemblies tested were made following ASTM D1002, with an overlapping area of 12.5 x 25 mm^2. The single lap shear (SLS) tests were performed on the Instron Universal 33R4204 tensile machine equipped with a 50 kN load cell with a crosshead speed of 2800 $N \cdot min^{-1}$ or 1 $mm \cdot min^{-1}$. The value of lap shear strength was calculated by Eq. 1.

$$LSS = \frac{F_{max}}{W_{area}} \quad (1)$$

In SLS test, the strength of a weld depends on the maximum load (F_{max}) at the breaking point divided by the real welded area (W_{area}) after failure.

Observations of the macrostructure and microstructure of surface for AA5083, the joint interface and fracture surfaces of AA5083-CF/PEKK joints were examined using a high-resolution optical microscope VHX-6000S by Keyence Corporation and a scanning electron microscope (SEM) with energy-dispersive X-ray spectroscopy (EDS) EVO HD 15 LS by ZEISS.

Results and Discussion

Morphology of the AA5083 substrate after laser treatment plays a significant role in joining since it promotes the mechanical interlocking of molten PEI into Al samples. At first, the influence of the roughness was studied. Fig. 2 shows the optical microscopy images of the prepared samples before and after mechanical treatments, polishing (SiC) P60 abrasive paper, as well as laser texturing. The roughness was measured using a roughness tester, a portable measuring device that determines the roughness depth (Ra, Rz, Rq and Rt). Thus, the roughness Ra for the raw material is 0.473 ± 0.012 µm, the mechanical polishing has created a surface roughness of 1.416 ± 0.198 µm, while the laser texturing allowed to obtain the average porosity of 5.521 ± 0.786 µm.

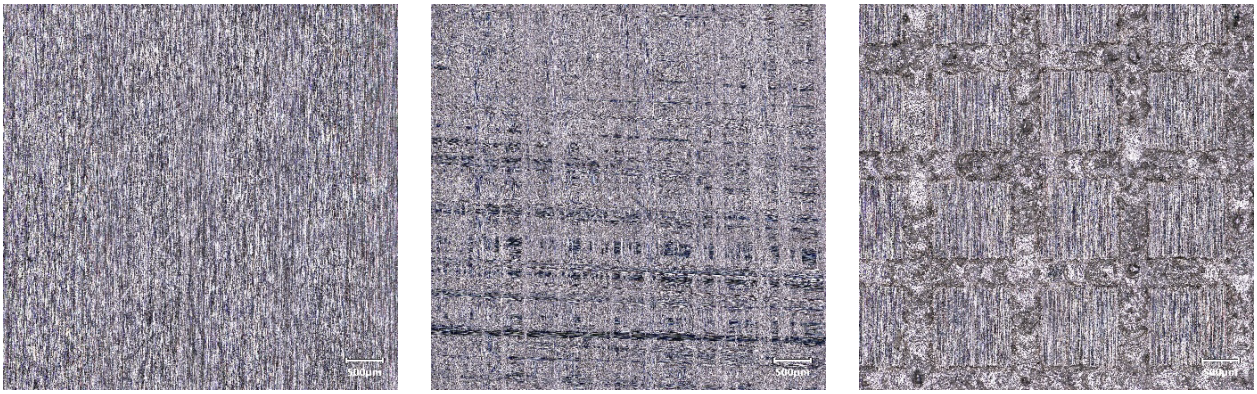

(a) (b) (c)

Fig. 2. Microstructure of (a) raw, (b) polished with P60 paper, (c) and laser-textured Al samples

To investigate the effect of laser texturing type on joint strength, the energy density is considered as constant. The grooves are clearly seen on the surfaces and recast layer, and burs are formed around texturing grid due to the melting of Al samples based on the 3D image from observations in Fig. 3. The grooves formed on the surface create a hierarchical structure. The depth scan line from optical microscope indicates that the molten aluminum deposits in the surface brings variations in the height of the walls and decreases the uniformity of the surface structure. Based on the groove depth measurements, the groove depth is less than 100 µm. Moreover, the aluminum deposition around edge of the laser path brings in depth fluctuation.

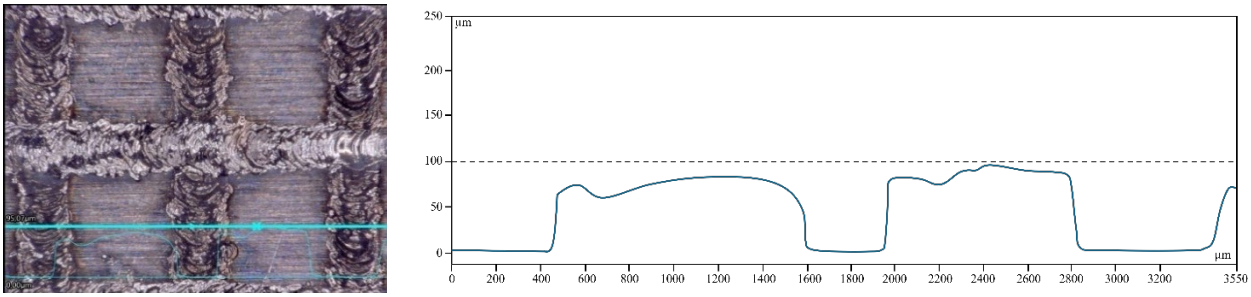

Fig. 3. Microstructure and groove depth of textured AA5083 sample

Preliminary ultrasonic welding tests revealed that laser-textured Al surfaces with an average roughness of 5.5 µm provided the most effective mechanical interlocking between the thermoplastic matrix and the metal substrate. Compared with raw Al samples and those manually abraded using

P60 abrasive paper, the laser-induced micro-channels and controlled periodic features significantly enhanced polymer flow and anchoring during welding. The improved interfacial morphology facilitated a more uniform wetting of the molten polymer and promoted stronger anchorage points, resulting in more stable welds. These findings confirm that precise, repeatable laser texturing yields a more favorable surface topography for metal-CF/PEKK hybrid joints than conventional mechanical abrasion or untreated surfaces.

Nevertheless, laser texturing of aluminum was found to be highly sensitive to the surrounding atmosphere, with noticeable differences between surfaces processed in atmospheric air and those textured under argon gas protection. When textured in atmospheric air, the high-energy laser pulses induced rapid local heating and selective oxidation of the alloying elements. Because magnesium has a much higher oxygen affinity than aluminum, the surface preferentially formed a magnesium oxide (MgO) layer, rather than aluminum oxide (Al_2O_3), Fig. 4.a. A significant amount of MgO becomes visible on the surface after the laser passes. This phenomenon is directly linked to the high local temperatures generated by the laser and the strong affinity of magnesium for oxygen. Magnesium has a lower boiling point (1090°C) and higher vapor pressure compared to aluminum, meaning that under intense heating, magnesium atoms tend to migrate toward the surface more readily. When the laser rapidly heats the alloy, often locally above 1500-2000°C, magnesium near the molten zone can segregate and diffuse upward to the surface. This MgO layer tended to be thicker, brittle, and uneven, and was often accompanied by micro-debris and irregular resolidified structures, which reduced the consistency of the textured features. Kim et al. [17] showed that when laser welding Al-Mg alloys in air, molecular spectra of MgO and AlO appear, whereas under argon shielding these oxide lines disappear. In contrast, laser texturing under an argon atmosphere strongly limited oxidation reactions, preventing the formation of MgO and leading to cleaner, sharper, and more uniform micro-grooves with improved reproducibility in depth and topography, Fig. 4.b. These atmospheric effects directly influence subsequent ultrasonic welding: argon-textured surfaces promote better polymer wetting and mechanical interlocking, while air-textured surfaces may hinder flow due to the presence of MgO and debris. Therefore, controlling the texturing atmosphere is essential to achieve high-quality surface functionalization for metal-CF/PEKK hybrid joints.

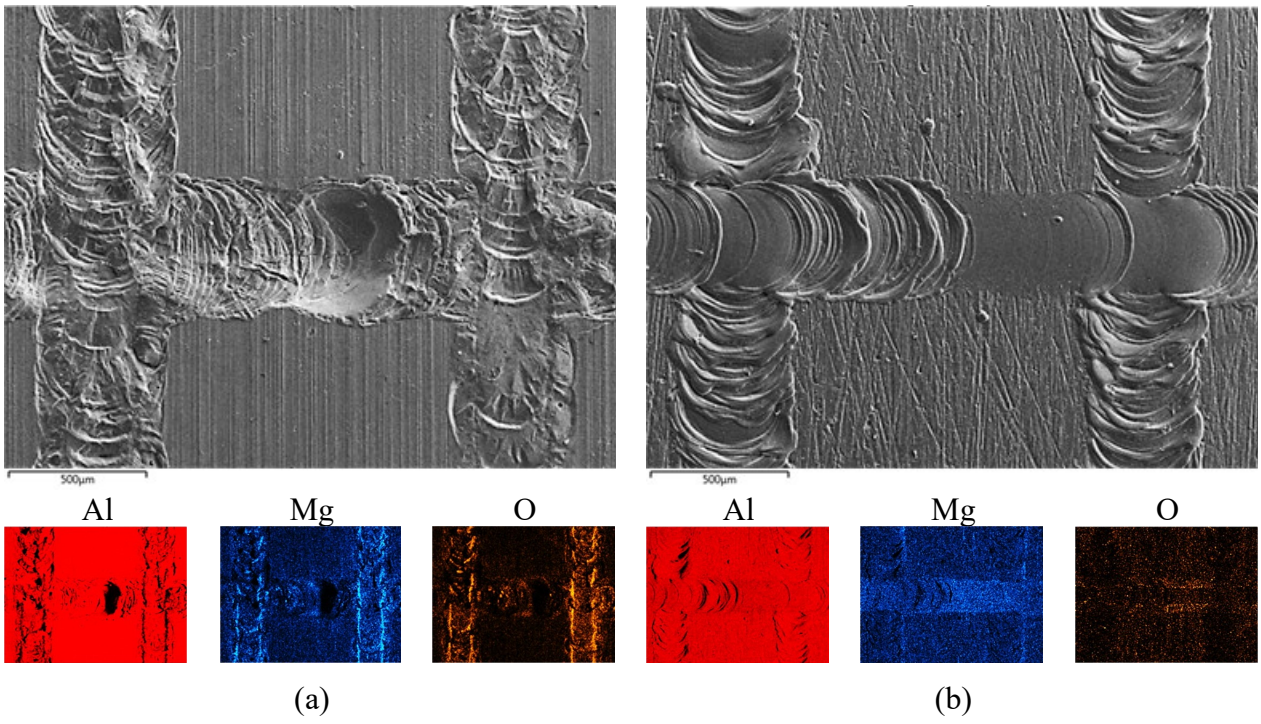

Fig. 4. Element map distribution of Al, Mg, O after laser texturing in (a) atmospheric air and (b) argon atmosphere

Performance of laser texturing under argon protection enabled the formation of well-defined micro-grooves that promoted an effective mechanical hook between the thermoplastic polymer and

the Al samples during ultrasonic welding. The argon atmosphere prevented oxidation during texturing, producing clean and sharp features that facilitated polymer flow and anchoring [18]. However, despite this improved mechanical interlocking, no significant chemical adhesion was observed at the metal-polymer interface, as the inert argon environment limits the formation of oxide (O^{2-}) species that could participate in interfacial bonding. To compensate for the absence of such functional surface chemistry, anodization of Al samples becomes necessary [19]. After laser texturing under argon, anodization is applied to improve the durability and strength of the bond. Here, the Al substrate is immerse in an acidic liquid, upon which an electric current is applied through substrate and liquid to enable an anodic corrosive reaction on the substrate surface. It generates a stable porous oxide layer capable of enhancing surface energy and providing chemical sites that improve polymer wetting and adhesion. Fig. 5.a presents anodized aluminum membranes created during chemical treatment, however when the image is zoomed, Fig 5.b, the nanopores reveal themselves. The thermoplastic can mechanically interlock inside these pores, which also results in an increased surface area. Consequently, combining argon-assisted laser texturing with subsequent anodization offers a promising route to achieve both strong mechanical interlocking and enhanced chemical bonding in hybrid metal-polymer joints.

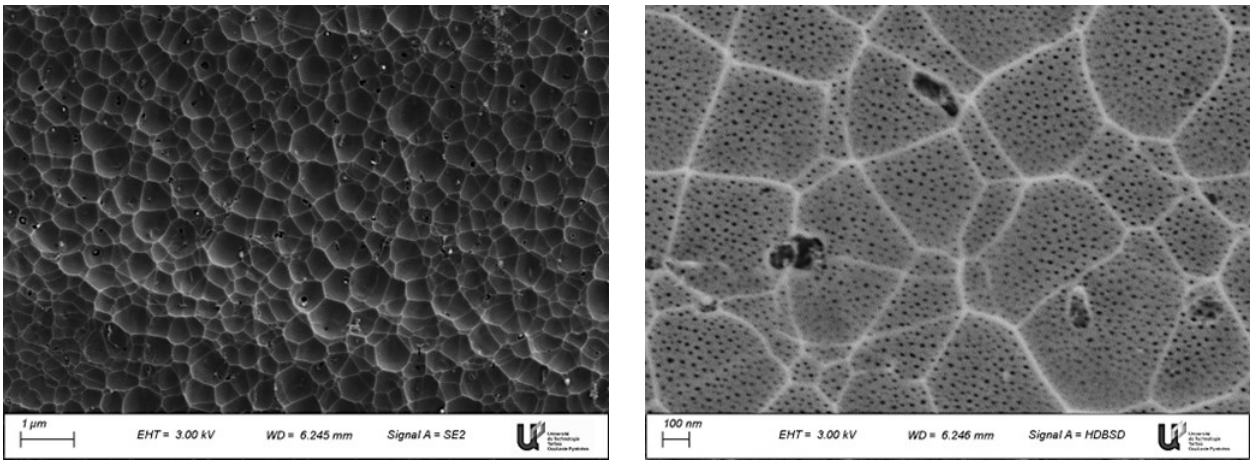

(a) (b)

Fig. 5. SEM images of the top view of (a) anodized aluminum oxide membrane with (b) enlarged pores

During sulphonic acid anodization of aluminum, the electrochemical process generates a porous alumina layer that contains incorporated sulfate (SO_4^{2-}) species originating from the electrolyte. These sulfur-containing groups become embedded within the anodic oxide and remain bound to the pore walls. The formation of porous anodic alumina via sulfuric-acid anodization can have beneficial effect of porous morphology on polymer adhesion [20]. However, the microstructure (porosity, pore density, pore diameter) depends strongly on the alloy composition, electrolyte, voltage, and processing parameters [21]. Such porous oxide layers generally enhance adhesion performance with polymers compared to bare aluminum, because the pores offer mechanical interlocking and improved wettability. For example, a recent study showed that optimizing anodized 6061 aluminum surface morphology improved bonding with carbon-fiber reinforced thermoplastics [20].

Polyetherimide (PEI), which contains imide groups (-CO-N-CO-) and aromatic rings, is known to interact more effectively with polar and high-energy surfaces. It is therefore hypothesized that sulfate-related species may contribute to increased surface polarity or acidity, potentially facilitating hydrogen bonding, van der Waals interactions, or dipole-dipole interactions with PEI. However, these specific interactions have not yet been experimentally confirmed and require further spectroscopic and interfacial characterization to be validated.

What is certain, based on established anodization behavior, is that the porous morphology of the anodic oxide enhances mechanical anchoring and improves wetting of molten PEI during ultrasonic welding. Any additional chemical contribution from sulfate species remains a promising but

unverified mechanism that warrants further study to fully understand and optimize metal-polymer adhesion.

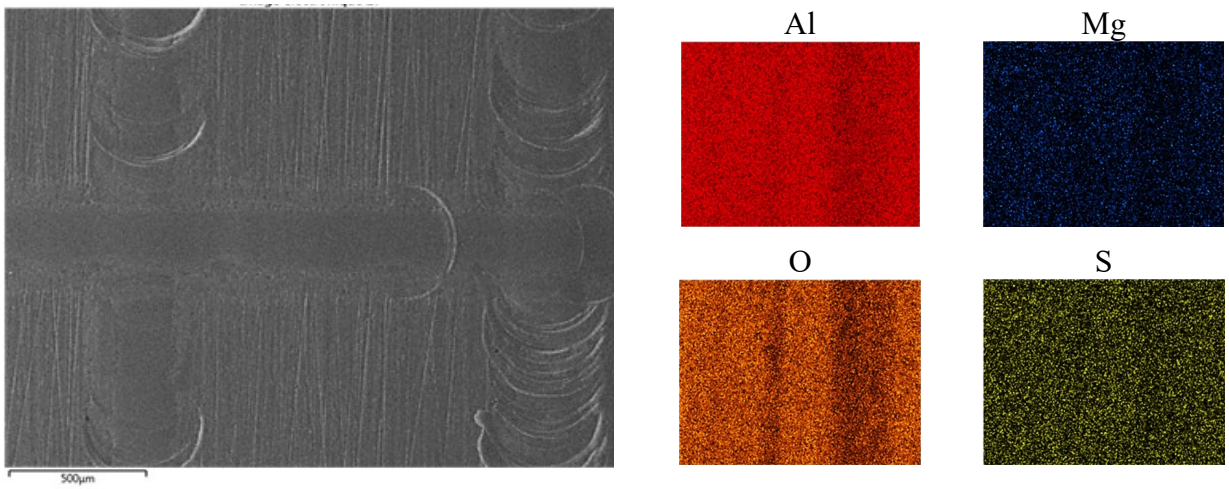

Fig. 6. Element map distribution of Al, Mg, O, S after laser texturing and anodization

Then, the ultrasonic welding parameters were established using a 40 mm diameter circular titanium sonotrode, drawing on insights from previous extensive trial-and-error optimization work. Key process variables responsible for heat generation at the interface, namely vertical pressure, vibration amplitude, and sonotrode displacement, were adjusted according to the specific material combinations. The innovative aspect of this study lies in the evaluation of a multi-mode ultrasonic welding strategy [22] and its influence on the mechanical performance of hybrid interfaces. Notably, most studies reported in the literature rely on a single control mode, limiting the flexibility and robustness of the process. In contrast, the controlled division of the vibration cycle employed here improves result reliability by automating and stabilizing the critical phases of the welding curve, which are essential for achieving high-quality, repeatable joints. In these experiments, the vibration phase was divided into three distinct stages, each using a different sonotrode amplitude.

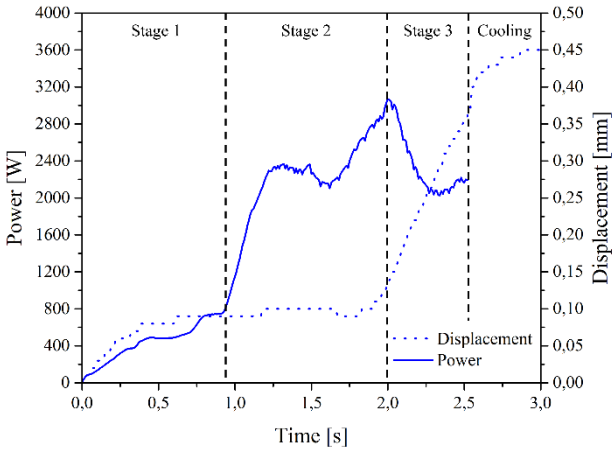

- Stage 1 (time-controlled mode) for 0.9 s with amplitude of 60 %
- Stage 2 (motion-detection mode) with an amplitude of 100 %
- Stage 3 (time-controlled mode) for 0.5 s with amplitude of 90 %
- Cooling phase with sonotrode displacement

Fig. 7. Power and displacement curves of ultrasonic welding for hybrid metal - polymer joints

The assemblies were kept under an operating pressure of 0.3 MPa during the welding process. A cooling time of 4 s at the operating pressure of 0.3 MPa was then applied. Fig. 7 presents the evolution of power and displacement during ultrasonic welding of the CF/PEKK using a PEI energy director against the aluminum substrate. The curve reveals four distinct welding phases, each corresponding to specific thermal-mechanical transformations at the joining interface. These phases determine the quality of the bond and the final mechanical performance of the welded joint.

In the first welding phase, ultrasonic power increases steadily while the sonotrode displacement remains low. At this point, heating is primarily driven by viscoelastic dissipation in the PEI energy director. PEI approaches its glass transition temperature and begins to soften, enabling intimate contact with both the CF/PEKK surface and the aluminum substrate. During this early phase, the PEKK matrix in the composite remains below its melting temperature, and the carbon fibers preserve their structural integrity. The aluminum substrate also behaves rigidly, undergoing only minor surface heating. This phase conditions the interface for efficient energy transfer and prepares the energy director for the onset of melting.

The second phase is characterized by a sharp increase in ultrasonic power, followed by the slow rise in displacement, indicating the onset of interfacial collapse. This corresponds to the flowing of the PEI energy director and partial softening of the PEKK matrix during the first peak of power with stable displacement. The molten PEI begins to flow laterally and vertically, filling microstructural features on the aluminum surface and initiating both wetting and diffusion of species.

Then, the second power peak appears when the entire PEI thickness of 0.25 mm has been flattened under the ultrasonic loading, marking the complete expulsion and redistribution of the softened energy director across the interface. Simultaneously, the CF/PEKK composite undergoes partial crushing of the surface plies, as the softened PEKK allows fiber imprints and local deformation. Together, these coupled phenomena when PEI collapse, aluminum flow, and surface crushing of CF/PEKK define the critical bonding window in which the final interfacial architecture and mechanical performance of the welded joint are established.

The final welding phase shows irregular power fluctuations accompanied by a rapid increase in displacement that gradually plateaus. This behavior reflects the final redistribution of molten PEKK within the aluminum surface features. At this moment the aluminum substrate also begins to experience flow localized on the corners under the combined effects of heat and pressure, which contributes to a more intimate contact with the molten polymer. As the interfacial layer collapses and consolidates, we assumed that a mixed PEI-PEKK interphase forms through molecular interdiffusion. The aluminum, regardless of texture or treatment, undergoes a little deformation on the corners of sample; its role is purely interfacial. In textured conditions, the grooves are progressively filled by the molten polymer, creating a mechanical hook. In anodized conditions, the role of oxide porosity, mechanical interlocking, and potential oxide-polymer interaction is possible [20], [23], [24]. The role of sulfate species in anodic alumina for PEI (or PAEK) adhesion remains a hypothesis. When the ultrasonic vibrations stop, the materials cool under pressure, resulting in solidification of the thermoplastics and stabilization of the final joint thickness.

After cooling, the joint exhibits a combination of mechanical interlocking, polymer-polymer entanglement between PEI and PEKK, surface chemical bonding in the presence of anodic sulphate-rich alumina and structural reinforcement from carbon fibers constraining the molten flow. This multi-mechanism consolidation explains the improved joint performance observed in optimized welding conditions.

The mechanical performance of the welded joints was evaluated through single lap shear testing, which revealed a LSS of 2.5 ± 1.7 MPa. However, the maximum LSS reached was 4.3 MPa. As comparison, the LSS of CF/PEEK welded with CF/PEEK can reach about 49 MPa [4]. This moderate strength reflects the combined effects of material behavior during welding and the interfacial architecture formed at the metal-polymer boundary. The relatively low LSS indicates that, although partial interfacial bonding was achieved, the total average welded zone was only 175 mm^2, instead of approximately 312 mm^2. The joint did not reach the levels typically expected for fully consolidated hybrid welds. The result suggests limitations in either polymer flow, mechanical interlocking, and/or chemical adhesion at the aluminum interface, consistent with the observed collapse behavior and incomplete wetting during the welding cycle.

The fractography of hybrid welded joints with aluminum substrate after single lap shear testing is presented in Fig. 8. The SEM images revealed clear evidence of PEI transfer onto the aluminum substrate (the black color in Fig.8.a), indicating partial interfacial adhesion developed during the welding process. The aluminum surfaces exhibited distinct patches and streaks of adhered PEI,

confirming that the molten energy director had sufficiently wetted the surface before solidification. In addition to polymer transfer, a very small but detectable transfer of aluminum into the PEI layer was observed (the white color in Fig. 8.b), suggesting that localized surface plasticization or micro-fragmentation occurred during the high-energy vibration phase. Furthermore, the fractured PEI surface displayed a well-defined imprint of the aluminum mesh pattern, demonstrating that the softened polymer was able to penetrate the surface micro-reliefs and form a mechanical hook during welding. This characteristic imprint confirms that mechanical interlocking contributes to the overall joint behavior. However, the discontinuous distribution of PEI residues and the limited extent of aluminum transfer correlate with the modest lap shear strength, indicating that adhesion occurred only in isolated zones rather than across a fully continuous interface.

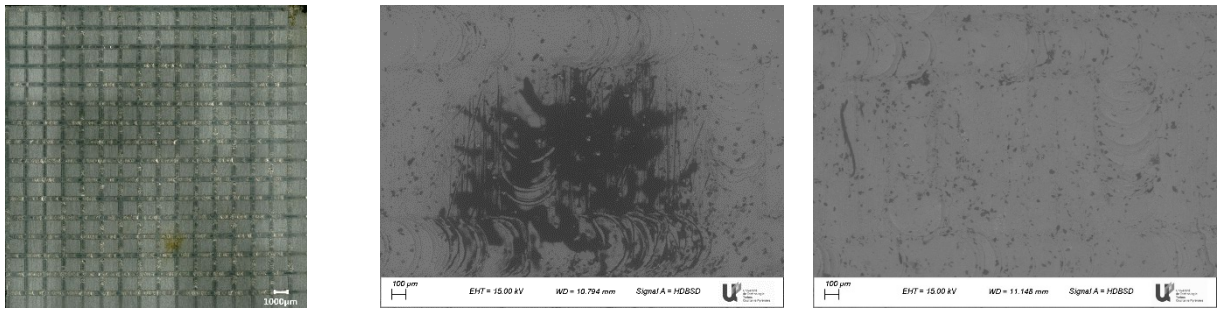

(a)

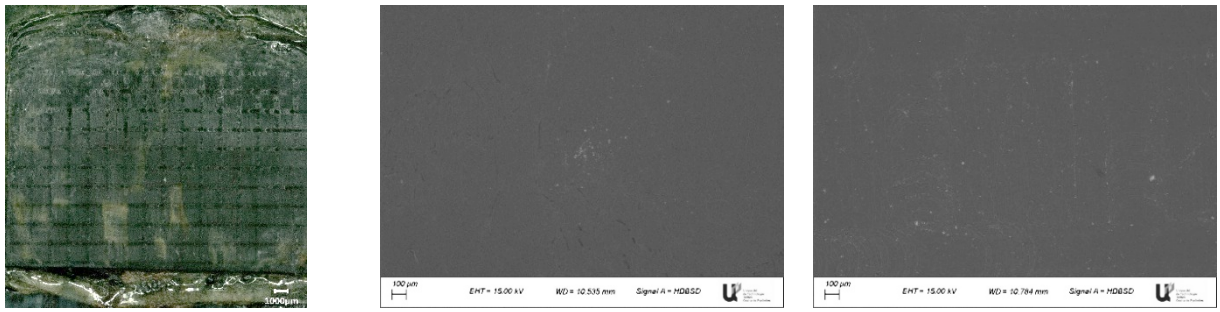

(b)

Fig. 8. Fractography of welded joints with SEM images for (a) aluminum substrate and (b) CF/PEKK substrate

Failure modes were predominantly interfacial, confirming that the adhesion mechanisms developed during welding were insufficient to sustain higher loads. These findings emphasize the need for improved surface preparation, enhanced energy director performance, and/or optimized ultrasonic parameters to achieve stronger and more reliable joints.

Summary

This study investigated the influence of aluminum surface finish and the use of a PEI energy director on the ultrasonic welding of PAEK/metal hybrid structures. The results demonstrate that surface preparation plays a decisive role in determining interfacial behavior, heat generation, and the resulting mechanical performance of the welded joints. Laser texturing under argon protection produced clean and well-defined micro-features that enabled effective polymer flow and mechanical interlocking, whereas laser texturing in ambient air promoted the formation of magnesium oxide, limiting wetting and reducing weld uniformity. Anodization further enhanced the interfacial chemistry by creating a porous, sulfate-rich oxide layer that improved PEI adhesion and contributed to more consistent polymer anchoring.

The use of a 0.25 mm PEI energy director facilitated controlled melting, polymer redistribution, and partial interdiffusion with the PAEK matrix, although the collapse behavior highlighted the sensitivity of the process to energy input and interface stability. Fractographic analyses revealed mixed adhesive-cohesive failure with limited PEI transfer and minor aluminum imprinting, indicating

that bonding occurred but remained discontinuous. As a result, the maximum measured lap shear strength of 4.3 MPa reflects the need for further optimization of interfacial design and welding parameters.

Overall, the study shows that ultrasonic welding of PAEK/metal hybrids is feasible, but its success strongly depends on the combination of surface morphology, surface chemistry, and energy director behavior. Future works should focus on improving oxide-layer engineering, refining laser texturing strategies, and developing tailored ED geometries to enhance both mechanical interlocking and chemical adhesion. These advances will help unlock the full potential of ultrasonic welding for high-performance hybrid structures in aerospace and other advanced engineering applications.

References

[1] F. Carassus, 'Le soudage par ultrasons des composites CF/PEEK en multimode et les propriétés de l'interphase d'un assemblage soudé', Doctorat Dissertations, University of Toulouse, Tarbes, France, 2024.

[2] F. Carassus, A. Korycki, C. Garnier, F. Chabert, M. Yahiaoui, and T. Djilali, 'Influence of Roughness in Ultrasonic Welding of Carbon Fiber/PEEK Composites', in *Materials Research Proceedings*, 2023, pp. 1841–1850. doi: 10.21741/9781644902479-199.

[3] A. Korycki, F. Carassus, C. Garnier, F. Chabert, and T. Djilali, 'Effect of Energy Director Thickness on Thermal Diffusion and Joint Quality during Ultrasonic Welding of CF/PEEK Composites', in *Materials Research Proceedings*, 2023, pp. 1819–1828. doi: 10.21741/9781644902479-197.

[4] M. Bonmatin, F. Chabert, G. Bernhart, T. Cutard, and T. Djilali, 'Ultrasonic welding of CF/PEEK composites: influence of welding parameters on interfacial temperature profiles and mechanical properties', *Composites Part A: Applied Science and Manufacturing*, vol. 162, no. 1, p. 107074_1–12, July 2022, doi: 10.1016/j.compositesa.2022.107074.

[5] A. Korycki, C. Garnier, F. Chabert, F. Carassus, and T. Djilali, 'Enhancing weld in ultrasonic spot welding of carbon fibre-reinforced polyetheretherketone with polyetherimide energy director', in *Materials Research Proceedings*, 2025, pp. 2273–2280. doi: 10.21741/9781644903599-245.

[6] M. Matus-Aguirre *et al.*, 'Laser Transmission Welding of PEKK: Influence of Material Properties and Process Parameters on the Weld Strength', in *Materials Research Proceedings*, 2023, Apr. 2023, pp. 1829–1840. doi: 10.21741/9781644902479-198.

[7] M. Villar Montoya *et al.*, 'In-situ infrared thermography measurements to master transmission laser welding process parameters of PEKK', *Optics and Lasers in Engineering*, vol. 106, no. 1, pp. 94–104, 2018.

[8] A. Korycki, C. Garnier, M. Bonmatin, E. Laurent, and F. Chabert, 'Assembling of carbon fibre/PEEK composites: comparison of ultrasonic, induction, and transmission laser welding', *Materials*, vol. 15, no. 6365, pp. 1–25, 2022.

[9] J. Molinar-Díaz, A. J. Parsons, I. Ahmed, N. A. Warrior, and L. T. Harper, 'Poly-Ether-Ether-Ketone (PEEK) Biomaterials and Composites: Challenges, Progress, and Opportunities', *Polymer Reviews*, vol. 65, no. 2, pp. 527–565, Apr. 2025, doi: 10.1080/15583724.2024.2406965.

[10] G. Wagner, F. Balle, and D. Eifler, 'Ultrasonic Welding of Aluminum Alloys to Fiber Reinforced Polymers', *Adv Eng Mater*, vol. 15, no. 9, pp. 792–803, Sept. 2013, doi: 10.1002/adem.201300043.

[11] R. Kalyan Kumar and M. Omkumar, 'Investigation of ultrasonic welding of carbon fiber reinforced thermoplastic to an aluminum alloy using a interfacial coating', *Materials and Manufacturing Processes*, vol. 36, no. 11, pp. 1323–1331, Aug. 2021, doi: 10.1080/10426914.2021.1905839.

[12] U. F. Dal Conte, I. F Villegas, and J. Tachon, 'Ultrasonic plastic welding of CF/PA6 composites to aluminium: Process and mechanical performance of welded joints', *Journal of Composite Materials*, vol. 53, no. 18, pp. 2607–2621, Aug. 2019, doi: 10.1177/0021998319836022.

[13] X. Tan *et al.*, 'Effect of laser texturing on mechanical strength and microstructure of ultrasonically welded ABS to aluminum alloy', *Journal of Materials Research and Technology*, vol. 31, pp. 3425–3435, July 2024, doi: 10.1016/j.jmrt.2024.07.057.

[14] F. Balle, G. Wagner, and D. Eifler, 'Ultrasonic Metal Welding of Aluminium Sheets to Carbon Fibre Reinforced Thermoplastic Composites', *Advanced Engineering Materials*, vol. 11, no. 1–2, pp. 35–39, 2009, doi: 10.1002/adem.200800271.

[15] S. T. Amancio-Filho, C. Bueno, J. F. dos Santos, N. Huber, and E. Hage, 'On the feasibility of friction spot joining in magnesium/fiber-reinforced polymer composite hybrid structures', *Materials Science and Engineering: A*, vol. 528, no. 10, pp. 3841–3848, Apr. 2011, doi: 10.1016/j.msea.2011.01.085.

[16] A. Korycki, F. Carassus, C. Garnier, F. Chabert, and T. Djilali, 'Effect of Consolidation Time in Hot Press Compression Molding of Continuous Carbon Fiber-Reinforced Polyetheretherketone Composite', *Polymer Composites*, vol. n/a, no. n/a, 2025, doi: 10.1002/pc.70717.

[17] J. D. Kim, J. S. Oh, M. H. Lee, and Y. S. Kim, 'Spectroscopic Analysis of Plasma Induced in Laser Welding of Aluminum Alloys', *Materials Science Forum*, vol. 449–452, pp. 429–432, 2004, doi: 10.4028/www.scientific.net/MSF.449-452.429.

[18] A. Al-Sayyad, J. Bardon, P. Hirchenhahn, R. Vaudémont, L. Houssiau, and P. Plapper, 'Influence of Aluminum Laser Ablation on Interfacial Thermal Transfer and Joint Quality of Laser Welded Aluminum–Polyamide Assemblies', *Coatings*, vol. 9, no. 11, p. 768, Nov. 2019, doi: 10.3390/coatings9110768.

[19] W. Zhao *et al.*, 'Enhanced bonding of polyphenylene sulfide-aluminum alloy composites using combined mild and hard anodizing techniques', *Surface and Coatings Technology*, vol. 483, p. 130773, May 2024, doi: 10.1016/j.surfcoat.2024.130773.

[20] L. Dong, Y. Li, M. Huang, X. Hu, Z. Qu, and Y. Lu, 'Effect of anodizing surface morphology on the adhesion performance of 6061 aluminum alloy', *International Journal of Adhesion and Adhesives*, vol. 113, p. 103065, Mar. 2022, doi: 10.1016/j.ijadhadh.2021.103065.

[21] I. Dobosz, 'Influence of the anodization conditions and chemical treatment on the formation of alumina membranes with defined pore diameters', *J Porous Mater*, vol. 28, no. 4, pp. 1011–1022, Aug. 2021, doi: 10.1007/s10934-021-01052-w.

[22] A. Korycki, C. Garnier, F. Chabert, F. Carassus, and T. Djilali, 'Enhancing weld in ultrasonic spot welding of carbon fibre-reinforced polyetheretherketone with polyetherimide energy director', in *Materials Research Proceedings*, 2025, pp. 2273–2280. doi: 10.21741/9781644903599-245.

[23] S. Li, H. Wan, J. Lin, and J. Min, 'Physicochemical interactions between amorphous metal oxide and polymer in metal–polymer hybrid materials', *Materials & Design*, vol. 230, p. 111993, June 2023, doi: 10.1016/j.matdes.2023.111993.

[24] S. W. Ryu, D. H. Kim, W. Lee, J.-Y. Hong, Y.-P. Jeon, and J. U. Lee, 'Improvement of Polymer/Metal Adhesion Using Anodizing Treatment and 3D Printing Process', *Polymers*, vol. 17, no. 3, p. 299, Jan. 2025, doi: 10.3390/polym17030299.